ELSEVIER

Polymer 43 (2002) 6027–6035

polymer

www.elsevier.com/locate/polymer

Mid-infrared optical properties of a polymer film: comparison between classical molecular simulations, spectrometry, and ellipsometry techniques

A. Soldera[a,*], E. Monterrat[b]

[a]*Département de Chimie, Chemistry Faculte des Sciences, Université de Sherbrooke, Sherbrooke, Que., Canada J1K 2R1*
[b]*CEA-LR, B.P. 16, 37260 Monts, France*

Received 24 April 2002; received in revised form 15 July 2002; accepted 16 July 2002

Abstract

Infrared optical properties of amorphous polymers, polymethylmethacrylate and polychlorotrifluoroethylene, are predicted following a procedure based on molecular simulation and Kramers–Kronig relations. The amorphous phase of polymer is first simulated with periodic boundary conditions. Normal mode vibrations and integrated intensities are then extracted from simulation data. These parameters allow the computation of the imaginary part, k, of the complex refractive index, N. Using Kramers–Kronig relations, the real part, n, of N, can be determined. The resulting spectrum is compared to spectra coming from two experimental techniques, spectrometry and ellipsometry. Three observations follow from such a comparison. Firstly, the ellipsometry is the most appropriate technique for this specific measurements. Secondly, some problems still exist in the intensity determination in the low frequency region. Thirdly, the mid-IR region is accurately depicted.

Keywords: Polymethylmethacrylate; Polychlorotrifluoroethylene; Refractive index

1. Introduction

Polymers are currently employed as materials for optical applications. Their high processability, their low cost and their ability to easily modify their properties by changing their chemical structure, are some of the factors that make polymers used in daily life. For instance, polymethylmethacrylate, PMMA, and poly-bis-phenol-A carbonate, PC, are employed when visible transparency is required (compact discs, headlights, etc.), and fluoride polymers are applied for a near infrared (IR) transparency (polymer optical fibers). However, to design a new polymer with specific optical properties, spectra have first to be computed. To achieve such calculations, two techniques are generally carried out: quantum chemistry and classical molecular modeling. Using the former technique, one can deal both with the electronic absorption that arises in the UV/visible region, and the molecular vibrations that occur in the infrared region. However, calculations are performed in systems containing a low number of atoms since they require a lot of central processing unit time. Nevertheless, if one is only concerned with vibrational spectroscopy, classical molecular modeling techniques that are mechanics and dynamics, are perfectly suitable, provided an accurate force field is used.

It has to be pointed out that the complex refractive indices are still unknown for most organic compounds [1]. Consequently, a complete procedure to determine these optical indices of a polymer prior to synthesizing it, is of great interest. However, the domain of validity of the procedure has to be clearly established. This is the reason why two experimental techniques, spectrometry and ellipsometry, are carried out on two polymers to compare their spectra with the simulated ones. Actually, data extracted from simulation can also be used to evaluate these experimental techniques.

2. Procedure

The optical properties of a polymer film are completely

* Corresponding author. Tel.: +1-819-8218000; fax: +1-819-8218017.
E-mail address: armand.soldera@usherbrooke.ca (A. Soldera).

0032-3861/02/$ - see front matter
PII: S0032-3861(02)00467-6

established when the real, n, and the imaginary, k, parts of the complex refractive index, N, are known all over the spectrum. The absorption, transmission and reflection spectra can thus be determined from molecular modeling data following the procedure exposed in this article, and summarized as follows:

1. molecular modeling of the selected polymer;
2. a drastic minimization;
3. extraction of the frequencies and the integrated intensities from simulation;
4. determination of the absorption coefficient, K, and therefore determination of the extinction coefficient, k;
5. calculation of n using the Kramers–Kronig relations;
6. computation of the reflection and transmission spectra using Fresnel formulae;
7. achieving the infrared absorption spectrum using the conversation law.

It has been shown that this procedure produces accurate infrared absorption spectra for two polymers, PMMA [2] and PCTFE (polychlorotrifluoroethylene) [3]. However, to completely determine the optical spectrum of a material the calculated refractive index, n, has to be reported with respect to the wavelength, and compared to experimental data. The experimental variations of n for the two polymers, PMMA and PCTFE, are investigated using two different techniques which are spectrometry and ellipsometry. With the former technique, the reflection and transmission spectra are first measured on a plastic film. n and k data are then calculated using a derivative method correlated with Fresnel formulae. With the latter technique, the n and k data come from the modulus, $\tan[\Psi(\tilde{\nu})]$, and the argument cosine, $\cos[\Delta(\tilde{\nu})]$, spectra of the complex reflection ratio, ρ. This parameter corresponds to the ratio between r_p and r_s, which are the parallel and the perpendicular reflection coefficients with respect to the incident plane, respectively.

3. Simulation of the polymer infrared spectra

The reliability of simulations is ultimately determined by the quality and accuracy of the force field employed. To calculate infrared spectra the second generation force field *pcff* from the Accelrys library is the best suited[1] since it possesses numerous cross-terms that are necessary to achieve an accurate calculated vibrational spectrum (Appendix A). These cross-terms depict the interactions of different internal coordinates [4]. It has to be mentioned that the non-bond parameters are best described using the COMPASS force field. However, calculations performed using this force field, do not clearly modify the final spectra. Only changes are observed in the final density.

All the calculations involving molecular modeling, steps 1–3 of the procedure, are performed using Accelrys software from InsightII 4.00 P environment. Steps 4–7 of the procedure, allowing the calculations of the real and imaginary parts of the refractive index, are incorporated into a macro command inside the Insight environment using BCL (biosym command language) commands with FORTRAN programs.

Table 1
Simulation data

Polymer	Initial density (g cm^{-3})	Final density (g cm^{-3})	Molar volume (cm^3 mol^{-1})	Refractive index
PMMA	1.17	1.11 ± 0.05	85.2	1.49
PCTFE	2.04	1.91 ± 0.07	57	1.42

It has to be pointed out that interferences are not taken into account in our calculations since the thickness of the polymer films used is in the order of 300 μm, and is clearly higher, by an order of magnitude, than the infrared wavelengths. Their complete treatment is described in MacLeod's book [5]. Nevertheless, they can be incorporated in the calculations through the introduction of an exponential term in the reflection and transmission coefficient terms, thus expressing the intensity decay. The different steps of the procedure are developed here below.

3.1. Simulation of the amorphous phase

The Accelrys *Amorphous_Cell*® software is used to simulate the polymer amorphous phase. The initial chain configuration is generated according to the propagation procedure implemented in the program. It is based on a combination of Theodorou and Suter's procedure [6] and Meirovitch's scanning method [7]. The chain backbone is grown step by step looking for long range excluded volume. In the Theodorou and Suter's model, the rotational isomeric states conditional probability [8], which is the probability to find the next bond of the backbone chain in a specific state, is modified to take into account the long range potential term. In the scanning method, all the possible continuations of the chain are theoretically looked at. In practice the lookahead is restricted to four bonds. Once the 'parent' polymer chain is built, it is embedded in a cubic cell whose volume is determined by the density and the molecular weight of the polymer. The actual densities both come from literature [9]. All the data useful for the simulation are displayed in Table 1. Periodic boundary conditions are then imposed to the system and, in order not to duplicate interactions, the minimum image convention is applied [10].

3.2. Minimization

After the amorphous polymer cell has been built, the *Discover_3*® software from MSI is used to perform molecular dynamics and mechanics calculations inside the cell. After the propagation procedure was carried out, a

[1] Discover_3® San Diego from Accelrys.

series of molecular dynamics simulations were performed. The purpose of such a series is not to reach the real density but to get the best occupancy of the cell by the polymer. For the two polymers, the same procedure was carried out. A first molecular dynamics simulation in the NVT ensemble, i.e. with constant number of particles, volume and temperature, is performed into the cell to relax the system during 10 ps. The integration step is 0.001 ps using the Verlet-leapfrog algorithm. The temperature is controlled with a Nose-Hoover thermostat bath [11,12]. The NPT ensemble, i.e. constant number of particles, pressure and temperature, is then chosen. The pressure was controlled with the Parrinello–Rahman algorithm [13]. Using such an ensemble allows the variation of the volume, and the density consequently. These simulations tend to approach experimental features. The duration of the molecular dynamics simulation is 100 ps. For both polymers, the final densities are shown in Table 1. As expected with the pcff force field, they are found lower than the experimental ones [14]. Actually, the final density does not have an impact on the final spectrum. Moreover, three polymer chains were generated and optimized following the procedure previously described. And the final spectra do not change significantly. Such an observation is in agreement with the fact that *pcff* force field was especially built to accurately reproduce the vibrational normal modes of polymers.

The molecular dynamics simulations are then followed by a series of energy minimization at constant volume: the steepest descent, the conjugate gradient, and the Newton–Raphson methods [15]. It has to be pointed out that the convergence criteria, which corresponds to the root-mean-square of the atomic derivatives for the energy, has to be very small, 10^{-5} kcal mol^{-1} Å^{-1}, in order for the vibrational frequencies to be correctly depicted (Eq. (1)) [16].

At the end of the minimization series the polymer conformation is in a locally energetic stable state within a uniformly occupied cell. As a consequence, the first energy derivative can be put equal to zero, and considering the harmonic approximation (terms higher than the second order are dismissed), only remains in the potential function expanded as a Taylor series, Eq. (1), the Hessian matrix. This matrix of force constants corresponds to the sum over each atom and its coordinates, of the second potential energy derivatives multiplied by small displacements [16].

$$V = V_0 + \sum_{i=1}^{3N}\left(\frac{\partial V}{\partial q_i}\right)_0 q_i + \frac{1}{2}\sum_{i=1}^{3N}\sum_{j=1}^{3N}\left(\frac{\partial^2 V}{\partial q_i \partial q_j}\right)_0 q_i q_j + \text{higher terms} \quad (1)$$

In Eq. (1), $q_i = \sqrt{m_\alpha}\Delta x_\alpha$ correspond to the mass-weighted cartesian displacement coordinates, where m_α indicates the mass of the atom α, and Δx_α, Δy_α, and Δz_α are the infinitesimal displacements of the coordinates according to the equilibrated nuclear position of the atom α; and 0 is a subscript corresponding to the equilibrated nuclear position.

3.3. Extraction of ν_i and S_i

It has to be mentioned that, since the harmonic approximation is considered, the overtones, the combination and the Fermi bands could not be seen in the final spectrum. The simulated molecule vibrational normal modes, ν_i, are extracted from the Hessian matrix, solving the secular equation [17]. Actually, the wavenumber, $\tilde{\nu}_i$, associated with the normal mode i, will be used instead of the frequency, ν_i. The simulation also gives another important vibrational parameter, the integrated intensity S_i associated with the normal mode i. Actually, S_i is computed from the dipole moment [18]

$$S_i = \frac{N_A \pi}{3c^2}\left(\frac{\partial \mu}{\partial q_i}\right)^2 \quad (2)$$

where N_A is the Avogadro's number, and c is the speed of light. A complete discussion on the vibration intensity can be found in Overend's chapter [18].

3.4. Determination of K and k

The absorption coefficient, $K(\tilde{\nu})$, associated with the wavenumber, $\tilde{\nu}$, is related to the imaginary part of the complex refractive index, k, which is generally called the extinction coefficient:

$$K(\tilde{\nu}) = 4\pi\tilde{\nu}k(\tilde{\nu}) \quad (3)$$

As the infrared beam progresses into the sample, if no scattering is considered, its intensity is reduced according to the Beer Lambert's law. As a matter of fact, the absorption coefficient of a sample can be written as:

$$K(\tilde{\nu}) = \frac{1}{x}\ln\left(\frac{I_0}{I}\right)_{\tilde{\nu}} \quad (4)$$

In this equation, I_0 and I are the intensities of the radiation before and after transmission by the sample, respectively. It has to be pointed out that x is the actual optical density absorption path length. It can thus be expressed as:

$$x = \rho_p e \quad (5)$$

In order to correctly depict the unit of the absorption coefficient, the polymer density, ρ_p, is substituted by the inverse of the polymer molar volume, V_m. This quantity is directly obtained from a QSPR [19] method, or from the Bicerano's analysis [20]. Its value for both polymers is displayed in Table 1. e is the absorption path length, so it is referred to the sample thickness.

Actually, from an empirically data analysis, isolated infrared extinction coefficient peaks conform fairly closely

to a Lorentzian line shape [21]

$$\ln\left(\frac{I_0}{I}\right)_{\tilde{\nu}} = \frac{a}{(\tilde{\nu} - \tilde{\nu}_0)^2 + b^2} \tag{6}$$

where a and b are constants. b is sometimes called the Lorentz or collision broadened half-width, and is equal to $\gamma/2$, where γ corresponds to the full-width-at-half-maximum, FWHM. Moreover, when $\nu = \nu_0$, i.e. the maximum of absorption is reached (ν_0 is the frequency at maximum absorption) $a/b^2 = [\ln(I_0/I)]_{\max}$.

In the present calculations, the FWHM, γ, is assumed to be constant all along the infrared spectrum, and its value is imposed to 20 cm^{-1}. According to the dispersion theory, γ is considered as the damping parameter, and cannot be easily computed.

Substitution of a and b by their respective values in Eq. (6), yields to the following expression:

$$\ln\left(\frac{I_0}{I}\right)_{\tilde{\nu}} = \left[\ln\left(\frac{I_0}{I}\right)\right]_{\max} \frac{\gamma}{4(\tilde{\nu} - \tilde{\nu}_0)^2 + \gamma^2} \tag{7}$$

The first term in the right-hand side (r.h.s) of Eq. (7) has to be determined. It is in fact related to the integrated absorption coefficient, i.e. the integrated intensity of a band. This intensity derives from simulation data as described in step 2 by Eq. (2) [17]. More generally, it has the following form [22]:

$$S = \int_{-\infty}^{+\infty} K(\tilde{\nu}) \mathrm{d}\tilde{\nu} \tag{8}$$

From substitution of the absorption coefficient in Eq. (4), by its Lorentzian form in Eq. (7), Eq. (8) becomes:

$$S = \frac{1}{x}\left[\ln\left(\frac{I_0}{I}\right)\right]_{\max} \gamma^2 \int_0^{+\infty} \frac{1}{4(\tilde{\nu} - \tilde{\nu}_0)^2 + \gamma^2} \mathrm{d}\tilde{\nu} \tag{9}$$

Solving Eq. (9) gives for the integrated intensity:

$$S = \frac{1}{x}\frac{\pi}{2}\gamma\left[\ln\left(\frac{I_0}{I}\right)\right]_{\max} \tag{10}$$

Merging Eqs. (4), (7) and (10), allows the determination of the absorption coefficient:

$$K(\tilde{\nu}) = \frac{2S}{\pi} \frac{\gamma}{4(\tilde{\nu} - \tilde{\nu}_0)^2 + \gamma^2} \tag{11}$$

Actually, all the parameters in the r.h.s of Eq. (11) are either extracted from the simulation, S and $\tilde{\nu}_0$, or imposed by the user, γ. As a matter of fact, this formula can be incorporated into a program, coupled with the simulation code.

Since the extinction coefficient, for a particular frequency, has the form of a Lorentzian function, it can be summed over all the normal modes i extracted from the Hessian matrix, and their corresponding integrated intensities, S_i. Therefore, Eq. (11) can be implemented in a program as:

$$K(\tilde{\nu}) = \sum_i \left[\frac{2S_i}{\pi} \frac{\gamma}{4(\tilde{\nu} - \tilde{\nu}_i)^2 + \gamma^2}\right] \tag{12}$$

For a particular frequency, the sum in Eq. (12) run all over the normal modes extracted from the Hessian matrix. As a matter of fact, $\tilde{\nu}_0$ from Eq. (11) is replaced by the wavenumber of the normal mode i, $\tilde{\nu}_i$. Such a calculation is carried out over a vibrational range. For instance, in our calculations, the domain begins at 500 cm^{-1} and finishes at 4000 cm^{-1}, with a step of 1 cm^{-1}.

At this stage of the procedure, the absorption coefficient spectrum is acquired. The imaginary part, k, of the refractive index is then directly deduced from such a spectrum since there exists a linear relation between the two parameters, as stated in Eq. (3).

3.5. Calculation of n

The real and imaginary parts of a response function are not independent when the function is causal. The causality condition actually corresponds to the fact that the output function cannot begin before the input function. The complex refractive index, N, meets such a requirement. As a result, since the imaginary part, k, of N, is known, the real part, n, of N, can be computed. This is effectively completed using the Kramers–Kronig relations [23].

$$n(\tilde{\nu}_i) - n(\infty) = \frac{2}{\pi} P \int_0^{\infty} \frac{\tilde{\nu} k(\tilde{\nu})}{\tilde{\nu}^2 - \tilde{\nu}_i^2} \mathrm{d}\tilde{\nu} \tag{13}$$

The integral in Eq. (13) runs all over the vibrational range previously defined. Moreover, to obtain the refractive index spectrum, this equation is computed for each frequency of this domain. Since for $\nu = \nu_i$, the integral is not defined, only the principal part of the integral, denoted by P, has to be calculated. Finally, it has to be pointed out that $n(\infty)$ represents the infinite frequency refractive index; as for the molar volume, it can be computed from QSPR [19] or Bicerano's [20] analysis. Its value for both polymers is displayed in Table 1. From a computing viewpoint, the integration inside Eq. (13) is performed using the MacLaurin's method.

The optical constants, i.e. the real, n, and imaginary, k, parts of the complex refractive index, N, are completely known all over the vibrational spectrum. Consequently, the computation of the reflection, transmission and absorption spectra can be achieved.

3.6. Computation of the reflection and transmission spectra

In order to correctly depict the experimental measurements, both faces of the polymer film are considered to be in contact with air. Moreover, the multiple reflection at both sample interfaces are introduced. As a consequence, according to the Fresnels formulae, the reflection and

transmission can be written as [5]:

$$R = R_i + \frac{T_i^2 T_p^2 R_i}{1 - T_p^2 R_i^2} \quad (14)$$

$$T = \frac{T_i^2 T_p}{1 - T_p^2 R_i^2} \quad (15)$$

R_i is the air/polymer interface reflection, it is directly obtained from the reflection coefficient, r: $R_i = rr^*$ with $r = (1 - N)/(1 + N)$, so $R_i = [(n - 1)^2 + k^2]/[(n + 1)^2 + k^2]$. T_i is the air/polymer interface transmission, $T_i = ntt^*$ with n the real part of the polymer refractive index and t, the transmission coefficient, $t = 2/(1 + N)$, so $T_i = 4n/[(1 + n)^2 + k^2]$. $T_p = \exp(-4\pi e k\tilde{\nu}/V_m)$ is the polymer internal transmittance. Interferences due to a low value of the film thickness, e, comparatively to the beam wavelength, can be introduced at this step of the procedure in the reflection and transmission coefficients [5].

3.7. Absorption spectrum

Finally, to compare simulated and experimental absorption infrared spectra, the absorption parameter, A, has to be computed. This is accomplished by considering the conservation law ($A = 1 - R - T$) where R and T correspond to the reflection and transmission spectra, respectively. Using such a procedure, the simulated spectra PMMA and PCTFE have shown an excellent agreement with experimental spectra [2,3].

4. Experimental part

Two kinds of experimental techniques have been run to extract the n and k spectra: spectrometry and ellipsometry.

- With the spectrometry technique, n and k values are deduced from the measurement of the R and T spectra through a plastic film, using a derivative method correlated with Fresnels formulae (Eqs. (14) and (15)). The R and T determination is performed at normal incidence (or quasi normal for R) in a 0.4–25 μm spectral range, employing a broadband Fourier transform infrared spectrometer (FTIR Bruker IFS88). For both kinds of measurement, a reference is needed. The reference spectrum for T corresponds to the background spectrum which is directly obtained from the measurement of the beam flow. Actually, the sample transmittance corresponds to the ratio of the reference flow and the flow passing through the sample. It has to be pointed out that the same acquisition parameters, i.e. resolution, slit aperture, and sampling frequency, have to be applied to both measurements. The reference spectrum for R is the reflection spectrum of a calibrated mirror (silver mirror for visible range, gold mirror for near and middle IR range). The same process as for transmittance measurement is then employed.
- Using the ellipsometry technique, the n and k data are derived from the $\tan(\Psi)$ and $\cos(\Delta)$ spectra which correspond to the modulus and the phase cosine of the reflection coefficient ratio, ρ, respectively. In order to acquire n and k values in a wide spectral range, two different devices have been used.
  - The first device is a Woollam variable angle spectroscopic ellipsometer (WVASE 32) operating in the 0.25–1.7 μm range. The wavelength is selected by a computer controlled grating monochromator. Using an optical fiber, the quasi-monochromatic light is guided from the monochromator to the sample surface, passing through a rotating polarizer. The reflected light beam, passing through a rotating analyzer, is then collected by one of the two detectors depending on the spectral range considered. In the 0.25–1 μm domain, the detector is a silicon diode, while in the 1–1.7 μm range, since the silicon becomes transparent the signal is detected by a InGaAs diode fixed behind it. Several measurements can be automatically performed at various angles. Those angles are generally selected in the 60–80° range, depending on the nature of the sample.
  - The second device is a Sopra VASE ellipsometer operating in the 1.5–17 μm domain. The difference with the previous device lies in the fact that the whole spectrum is acquired in one scan only using a FTIR (Bruker IFS25). However, several scans are required to improve the signal-to-noise ratio. Actually, no optical fiber is necessary since the spectrometer exit window is in the ellipsometer optical path. After passing through a rotating analyzer, the reflected light beam is focused on the Mercury Cadmium Telluride detector window by a spherical mirror. The main advantage of ellipsometry in comparison with the spectrometry is that no reference is needed. For each wavelength the measured value corresponds to the ratio of the sample surface reflection coefficient in the two polarization directions. The two spectra thus acquired are, in fact, the Fourier coefficients, α and β, of the $2A$ harmonic (A is the angle of the analyzer) which allow the determination of $\tan[\Psi(\tilde{\nu})]$ and $\cos[\Delta(\tilde{\nu})]$, without the need of the absolute intensity (Appendix B) [24].

For the two techniques, the calculations allowing the determination of the n and k spectra are exposed in Appendix B.

5. Results and discussion

The real parts of the complex refractive index simulated

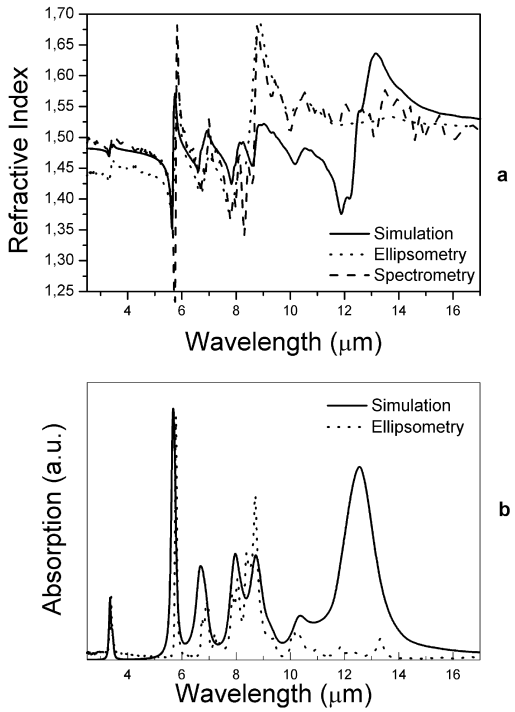

Fig. 1. Comparison between simulated and experimental real part, n, of the complex refractive index N (a) and absorption (b) spectra of PMMA.

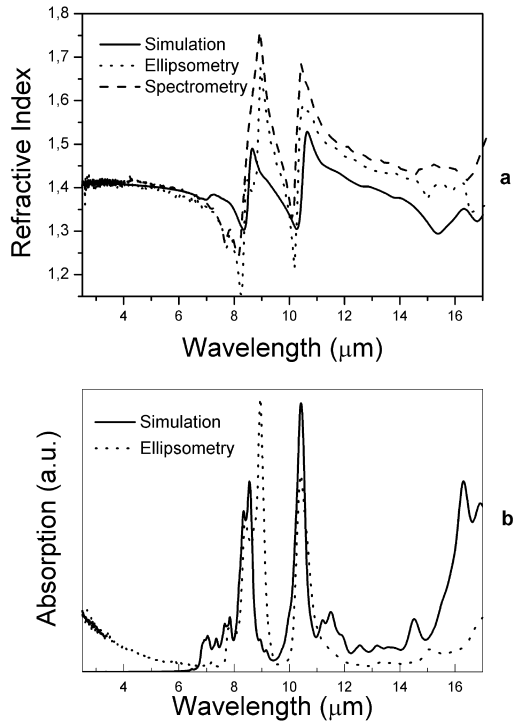

Fig. 2. Comparison between simulated and experimental real part, n, of the complex refractive index N (a) and absorption (b) spectra of PCTFE.

spectra are compared to the experimental spectra resulting from spectrometric and ellipsometric measurements, for the two polymers, PMMA and PCTFE, in Figs. 1(a) and 2(a), respectively. The simulated and experimental absorption spectra of PMMA and PCTFE are shown in Figs. 1(b) and 2(b), respectively. The vibrational calculation and the ellipsometer apparatus impose the lower (2.5 μm–4000 cm^{-1}) and upper (17 μm–588 cm^{-1}) limits of the infrared spectrum. It has to be pointed out that in the spectrum originating from spectrometric measurement, the region of the absorption peaks has a lack of points. The reason for such a behavior is that derivative methods are employed to compute n and k. As a matter of fact, the absorption spectra originating from such a device are not displayed in Figs. 1(b) and 2(b). The detail of the calculation is presented in Appendix B.

Both polymers show an accurate agreement between calculated and experimental spectra of the refractive index. As a consequence, a good accuracy is achieved for the simulated absorption spectra. The normal modes are correctly described indicating the quality of the force field, *pcff*, and the correctness of the procedure. However, some discrepancies in intensities between experimental and simulated spectra exist in the high wavelength domain (low frequencies). To explain such a difference, we first looked at the effect of the γ variation on the spectrum. Since γ corresponds to the damping parameter in the dispersion theory (or the FWHM in the Lorentz function), some deductions resulting from location of vibrational modes on the spectrum can be obtained. The stretching vibrations are mainly located in the high frequency region. As a result, they are less restrained, i.e. they possess less degrees of freedom than wagging vibrations mainly located in the low frequency region. Therefore, wagging vibrations exhibit a higher value of γ than the stretching vibrations do. Since the absorption coefficient decreases with a higher value of γ, simulated intensities at low frequencies are lower than the experimental ones. Actually, this reduction is not important, and cannot alone explain such a difference in the intensities at low frequencies between experimental and simulated spectra. Another explanation stays in the harmonic oscillator approximation used in developing the dipole moment in a Taylor series in terms of the normal coordinates [16]:

$$\mu = \mu_0 + \sum_{i=1}^{3N} \frac{\partial \mu}{\partial q_i} q_i + \text{higher terms} \tag{16}$$

Using the harmonic approximation, only the constant and linear terms remain in Eq. (16), the higher terms are neglected. From a quantum mechanical description of infrared absorption, this leads to the equation of the integrated intensity, Eq. (2). The dipole moment second derivative was primarily thought to have an influence on the final intensity at the low frequency region. But, according to Overend, the introduction of $\partial^2 \mu / \partial q_i^2$ in the intensity term of the fundamental band, does not have major effect [18].

Some simulation parameters were then changed to

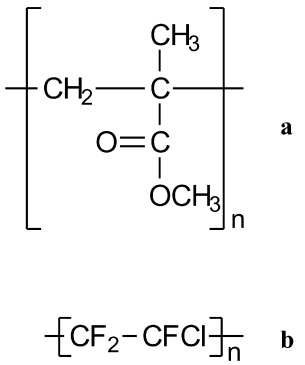

Fig. 3. Chemical formulae of PMMA (a) and PCTFE (b) monomers.

observe their impact on the final spectra. Since no significant modifications were observed, no data were reported. Different partial charges, computed using charge equilibration approach [25], were used. The length of the polymer chain was also changed without any success. Actually, the vectors associated with the normal modes located in the high frequency region show a collective motion of all the chain. Consequently, a small coordinate displacement involves a great variation of the overall dipole. As a matter of fact, according to Eq. (2), this will give rise to a high intensity. Further studies are presently done to get acquainted with such a behavior.

However, other effects on intensity coming from the fact that the infrared spectra are computed in a condensed phase, are difficult to take into account. Actually, calculation of intensity using force fields is still a troublesome task. Nevertheless, the vibrations overall the spectrum are accurately depicted, and the intensities are accurately reproduced in the mid-IR region (2–12 μm) [1].

From a general viewpoint, the simulated spectra have been compared to experimental ones. Some differences exist between the behavior of the two plastic spectra. The PCTFE calculated spectrum presents a better accuracy to the experimental spectra than PMMA does. Such a difference can be explained from a microscopic and macroscopic viewpoints. Intrinsically, the PCTFE monomer exhibits a simple structure compared to the PMMA monomer (Fig. 3(a) and (b)). As a matter of fact, it displays a smaller number of normal modes. Extrinsically, the PCTFE film is flexible while PMMA shows a glass transition temperature higher than the ambient temperature (around 100 °C for the *at*-PMMA). Actually, using an ellipsometer apparatus, the more the upper and lower faces of a film are parallel, the more reflections can arise. As a consequence, using a more rigid film, like the PMMA film, involves an increase of the reflections as can be observed in Fig. 2.

Finally, some comments about experimental techniques arise from the comparison between simulated and experimental data. In the low wavelength region, simulated data are more accurately correlated with ellipsometric measurements than with spectrometric ones, it is in fact especially observed for PMMA. This is in accordance with the fact that, for our kind of samples, the ellipsometry is more appropriate than spectrometry since no reference is needed, and semi-infinite medium is considered. With spectroscopy, the measurement is performed on a flow ratio. Actually, it is the easiest way to carry out such an analysis. However, references have to be employed: for transmittance determinations, the reference is the air, while for reflectance determinations, a mirror has to be used. Consequently, the reflectance level decreases with time due to handling and atmosphere. As a matter of fact, experimental errors increase. Such a problem is not observed with ellipsometric measurement. The $\tan[\Psi(\tilde{\nu})]$ and $\cos[\Delta(\tilde{\nu})]$ spectra, the actual Fourier coefficients α and β (Appendix B), are obtained from the ratio of reflected intensities with different polarization configurations, i.e. with different polarizer and analyzer positions. The sample and the optical path do not change.

Consequently, simulated results in the mid-IR region are in perfect agreement with the experimental data coming from the ellipsometry technique, which is the most appropriate device for our particular use. Further infrared analysis can therefore be carried out running the exposed procedure.

6. Conclusion

The procedure presented in this text allows the computation of the optical properties, that are the real, n, and imaginary, k, parts of the complex refractive index, N, of an amorphous polymer. The excellent agreement in the mid-IR region between simulated and experimental data, show the accuracy of the procedure used, and the precision of the force field, *pcff*. As pointed out by Wang et al. [1], the complex refractive indices are still unknown for most organic compounds. Therefore, using the procedure exposed, and considering the accuracy accomplished, unknown refractive indices of polymers can be computed.

However, low frequency intensities are still overestimated. To solve this problem, molecular dynamics simulation can be run, instead of molecular mechanics calculation used in our present work [26]. From such a simulation, the dipole autocorrelation function is computed. Thereafter, the Fourier transform is performed and the infrared spectrum is obtained [27]. Some discrepancies still exist in intensities for longer wavelength, but studies are currently carried out to better understand this behavior.

Finally, from a comparison with simulation, the ellipsometry technique is more appropriate than the spectrometric technique for our specific measurements.

Appendix A

Energy expression of the pcff force field

$$V = \sum_b [K_2(b-b_0)^2 + K_3(b-b_0)^3 + K_4(b-b_0)^4] + \sum_\theta [H_2(\theta-\theta_0)^2 + H_3(\theta-\theta_0)^3 + H_4(\theta-\theta_0)^4] + \sum_\phi [V_1[1-\cos(\phi-\phi_1^0)] + V_2[1-\cos(2\phi - \phi_2^0)] + V_3[1-\cos(3\phi-\phi_3^0)]] + \sum_\chi K_\chi \chi^2 + \sum_b \sum_{b'} F_{bb'}(b-b_0)(b'-b_0') + \sum_\theta \sum_{\theta'} F_{\theta\theta'}(\theta - \theta_0)(\theta'-\theta_0') + \sum_b \sum_\theta F_{b\theta}(b-b_0)(\theta-\theta_0) + \sum_b \sum_\phi (b-b_0)[V_1\cos\phi + V_2\cos 2\phi + V_3\cos 3\phi] + \sum_{b'} \sum_\phi (b'-b_0')[V_1\cos\phi + V_2\cos 2\phi + V_3\cos 3\phi] + \sum_\theta \sum_\phi (\theta-\theta_0)[V_1\cos\phi + V_2\cos 2\phi + V_3\cos 3\phi] + \sum_\phi \sum_\theta \sum_{\theta'} K_{\phi\theta\theta'}\cos\phi(\theta-\theta_0)(\theta'-\theta_0') + \sum_{i>j} \frac{q_i q_j}{\varepsilon r_{ij}} + \sum_{i>j}\left[\frac{A_{ij}}{r_{ij}^9} - \frac{B_{ij}}{r_{ij}^6}\right] \quad \text{(A1)}$$

where $K_2, K_3, K_4, H_2, H_3, H_4, V_1, V_2, V_3$, $K_\chi, F_{bb'}, F_{\theta\theta'}, F_{b\theta}$, and $K_{\phi\theta\theta'}$ are the force field parameters; b and b', the bond lengths; b_0 and b_0', the reference values of the corresponding bond length; θ and θ', the bond angles; θ_0 and θ_0', the reference values of the corresponding bond angle; ϕ, a torsion angle; ϕ_1^0, ϕ_2^0, and ϕ_3^0, the reference values of the corresponding torsion angle; q_i and q_j, the atomic partial charges on atoms i and j; r_{ij}, the distance between them; ε, the dielectric constant and A_{ij} and B_{ij} are the force field parameters.

Appendix B

B.1. Spectroscopic (R and T) measurements

R and T are functions of n and k. It has to be noted that they are also functions of the beam wavelength, λ, since n and k have been expressed as functions of the wavenumber. As a result, R and T can be differentiated by n and k, giving two equations with two unknown parameters that are ΔR and ΔT

$$\Delta R = \frac{\partial R}{\partial n}\Delta n + \frac{\partial R}{\partial k}\Delta k \quad \text{(B1)}$$

$$\Delta T = \frac{\partial T}{\partial n}\Delta n + \frac{\partial T}{\partial k}\Delta k \quad \text{(B2)}$$

where ΔR and ΔT are the numerical differences between the calculated and the experimental values of reflection and transmission, respectively, while Δn and Δk are the numerical differences between the computed current values and the expected values. This system can be inverted to get the expression of Δn and Δk as functions of ΔR, ΔT and the partial derivatives of R and T.

If the sample faces are parallel, which is the most current case, multiple reflections have to be taken into account within the sample thickness. In this work, the polymer films are sufficiently thick compared to the beam wavelength to neglect the interference phenomena. R and T are then expressed in Eqs. (14) and (15).

The air/polymer internal reflection, R_i, air/polymer interface transmission, T_i, and the polymer internal transmittance, T_p, are expressed as functions of n and k:

$$R_i = \frac{(n-1)^2 + k^2}{(n+1)^2 + k^2} \quad \text{(B3)}$$

$$T_i = \frac{4n}{(n+1)^2 + k^2} \quad \text{(B4)}$$

$$T_p = \exp\left(-4\pi k \frac{e}{V_m}\frac{1}{\lambda}\right) \quad \text{(B5)}$$

Once the measurements of R and T have been performed, an iterative procedure to calculate n and k is initiated. The first step consists in choosing judicious values for n and k, at the beginning of the spectrum ($\lambda = 0.4\ \mu m$). The iterative calculation is then carried out in order to achieve $\Delta R^2 + \Delta T^2 < \varepsilon$, where ε is set to 10^{-8}. The number of iterations is generally comprised between 5 and 10. For each sequenced wavelength, the calculation begins with n and k values previously obtained. Such a calculation gives a spectrum after a few seconds.

The major problem ensuing from this kind of numerical extraction is to measure R and T with a rather high signal to noise ratio. In fact, when T is close to zero, the n and k values cannot be extracted using derivatives in Eqs. (B1) and (B2). As a matter of fact, this method is particularly convenient for materials which are transparent in this spectral range.

B.2. Ellipsometric measurements

The electric field is split into a perpendicular, S wave, and a parallel, P wave, components according to the incident plane. When a beam is reflected on a sample surface, its polarization state is modified. The two waves exhibit different behavior after the reflection occurs on the surface. As a matter of fact, there are two reflection coefficients, r_p

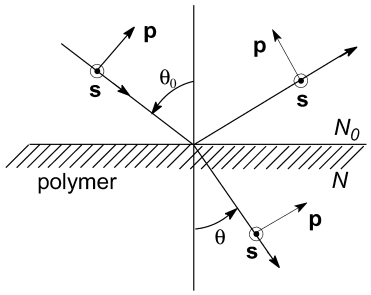

Fig. 4. Schematic representation of reflection on a plastic medium, in an ellipsometry apparatus.

and r_s, according to the S and P waves, respectively. The change in the polarization state is characterized by the ratio of these two reflection coefficients, ρ. This ratio is commonly expressed as:

$$\rho = \frac{r_p}{r_s} = \tan(\Psi)\exp(j\Delta) \tag{B6}$$

The form of ρ in Eq. (B6) allows the separation of its modulus, $\tan(\Psi)$ and its cosine phase, $\cos(\Delta)$ Actually, ellipsometric measurements are performed on a sample where the reflection only comes from the first interface (air–material). As a matter of fact, the medium is considered to be semi-infinite. For instance, the medium can be a thick material with the rear face etched or with two non-parallel faces. ρ can thus be calculated from the complex refractive indexes of the two media, N_0 and N, the incident angle, θ_0, and the Fresnel equations associated with the reflection coefficients, r_p and r_s, expressed in Eqs. (B7) and (B8), respectively. A semi-infinite medium is depicted in Fig. 4. It has to be pointed out that considering a semi-infinite medium amounts to saying that the second term of the r.h.s. of Eq. (14) is zero, thus $R = R_i$.

$$r_p = \frac{N\cos(\theta_0) - N_0\cos(\theta)}{N\cos(\theta_0) + N_0\cos(\theta)} \tag{B7}$$

$$r_s = \frac{N_0\cos(\theta_0) - N\cos(\theta)}{N_0\cos(\theta_0) + N\cos(\theta)} \tag{B8}$$

The θ angle is established according to the Snell–Descartes relation: $N_0\sin(\theta_0) = N\sin(\theta)$. From Eqs. (B7) and (B8), an expression of N is obtained:

$$N^2 = N_0^2\sin^2(\theta_0)\left[1 + \left(\frac{1-\rho}{1+\rho}\right)^2\tan^2(\theta_0)\right] \tag{B9}$$

If the incident medium is air (which is generally the case), $N_0 = 1$. Since ρ is a complex quantity, the n and k values are simultaneously determined from Eq. (B9).

Actually, to measure $\tan(\Psi)$ and $\cos(\Delta)$, different kinds of ellipsometer arrangements exist. The apparatus which has been used for the measurements presented in this paper, is based on the rotating-analyzer ellipsometer [24]. The sample is placed between rotating polarizer and analyzer. The detected intensity at the angle A of the analyzer is then written as

$$I(A) = I_0[1 + \alpha\cos(2A) + \beta\sin(2A)] \tag{B10}$$

where I_0 is the absolute intensity, and α and β are the Fourier coefficients of the $2A$ harmonic. These two parameters yield to the ellipsometric components, $\tan(\Psi)$ and $\cos(\Delta)$

$$\tan(\Psi) = \tan(P)\sqrt{\frac{1+\alpha}{1-\alpha}} \tag{B11}$$

$$\cos(\Delta) = \frac{\beta}{\sqrt{1-\alpha^2}} \tag{B12}$$

where P is the polarizer angle. According to the analyzer angle, α and β are measured, and they thus allow the determination of $\tan(\Psi)$ and $\cos(\Delta)$, without the need of the absolute intensity measurement.

References

[1] Wang Y, Abe Y, Matsuura Y, Miyagi M, Uyama H. Appl Opt 1998; 37:7091–5.
[2] Soldera A, Dognon JP. Macromol Symp 1997;119:157.
[3] Soldera A. Macromol Symp 1998;133:11–20.
[4] Gelin BR. Molecular modeling of polymer structures and properties. Munich: Hanser; 1994.
[5] Macleod HA. Thin-film optical filters. London: McGraw-Hill; 1989.
[6] Theodorou DN, Suter UW. Macromolecules 1985;18:1467–78.
[7] Meirovitch H. J Chem Phys 1983;79(1):502–8.
[8] Flory PJ. Statistical mechanics of chain molecules. New York: Hanser; 1989.
[9] Brandrup J, Immergut EH. Polymer handbook. New York: Wiley/ Interscience; 1989.
[10] Allen MP, Tildesley DJ. Computer simulation of liquids. Oxford: Clarendon Press; 1987.
[11] Nosé S. J Chem Phys 1984;81:511.
[12] Hoover WG. Phys Rev A 1985;31:1695.
[13] Parrinello M, Rahman A. J Appl Phys 1981;52:7182.
[14] Sun H. J Phys Chem B 1998;102:7338–64.
[15] Burkert U, Allinger NL. Molecular mechanics. Washington: ACS; 1982.
[16] Painter PC, Coleman MM, Koenig JL. The theory of vibrational spectroscopy and its application to polymeric materials. New York: Wiley; 1982.
[17] Wilson EBJ, Decius JC, Gross PC. Molecular vibrations: the theory of infrared and Raman vibrational spectra. New York: Dover; 1980.
[18] Overend J. IR spectroscopy and molecular structure; 1963. p. 345.
[19] Van Krevelen DW. Properties of polymers. Amsterdam: Elsevier; 1990.
[20] Bicerano J. Prediction of polymer properties. New York: Marcel Dekker; 1993.
[21] Bower DI, Maddams WF. The vibrational spectroscopy of polymers. Cambridge: Cambridge University Press; 1989.
[22] Bertie JE, Zhang SL, Keefe CD. J Mol Struct 1994;324:157–76.
[23] Yamamoto K, Ishida H. Vib Spectrosc 1994;8:1–36.
[24] Azzam RMA, Bashara NM. Ellipsometry and polarized light. Amsterdam: Elsevier; 1987.
[25] Rappé AK, Goddard WA. J Phys Chem 1991;95:3358.
[26] Dumont D, Bougeard D. Comput Theor Polym Sci 1999;9:87–9.
[27] Tiller AR. Macromolecules 1992;25:4605–11.